23

Synthesis and X-Ray Crystal Structure of α-Keggin-Type Aluminum-Substituted Polyoxotungstate

Chika Nozaki Kato[1], Yuki Makino[1], Mikio Yamasaki[2], Yusuke Kataoka[3], Yasutaka Kitagawa[3] and Mitsutaka Okumura[3]

[1]*Shizuoka University*
[2]*Rigaku Corporation*
[3]*Osaka University*
Japan

1. Introduction

Aluminum and its derivatives such as alloys, oxides, organometallics, and inorganic compounds have attracted considerable attention because of their extreme versatility and unique range of properties, including acidity, hardness, and electroconductivity (Cotton & Wilkinson, 1988). Since the properties and activities of an aluminum species are strongly dependent on the structures of the aluminum sites, the syntheses of aluminum compounds with structurally well-defined aluminum sites are considerably significant for the development of novel and efficient aluminum-based materials. However, the use of these well-defined aluminum sites is slightly limited by the conditions resulting from the hydrolysis of the aluminum species by water (Djurdjevic et al., 2000; Baes & Mesmer, 1976; Orvig, 1993; Akitt, 1989).

Polyoxometalates have been of particular interest in the fields of catalytic chemistry, surface science, and materials science because their chemical properties such as redox potentials, acidities, and solubilities in various media can be finely tuned by choosing appropriate constituent elements and countercations (Pope, 1983; Pope & Müller, 1991, 1994). In particular, the coordination of metal ions to the vacant site(s) of lacunary polyoxometalates is one of the most effective techniques used for constructing efficient and well-defined active metal centers. Among various lacunary polyoxometalates, a series of Keggin-type phosphotungstates is one of the most useful types of lacunary polyoxometalates. Fig. 1 shows some examples of lacunary Keggin-type phosphotungstates, i.e., *mono*-lacunary α-Keggin $[\alpha\text{-}PW_{11}O_{39}]^{7-}$ (Contant, 1987), *di*-lacunary γ-Keggin $[\gamma\text{-}PW_{10}O_{36}]^{7-}$ (Domaille, 1990; Knoth, 1981), and *tri*-lacunary α-Keggin $[A\text{-}\alpha\text{-}PW_9O_{34}]^{9-}$ (Domaille, 1990) phosphotungstates. Knoth and co-workers first synthesized the Keggin derivative $(Bu_4N)_4(H)ClAlW_{11}PO_{39}$ by the reaction of *mono*-lacunary α-Keggin phosphotungstate with $AlCl_3$ in dichloroethane (Knoth et al., 1983). However, only a few aluminum-coordinated polyoxometalates (determined by X-ray crystallographic analysis) have been reported, e.g., a monomeric, *di*-aluminum-substituted γ-Keggin polyoxometalate $TBA_3H[\gamma\text{-}SiW_{10}O_{36}\{Al(OH_2)\}_2(\mu\text{-}$

$OH)_2]\cdot 4H_2O$ (TBA = tetra-*n*-butylammonium) (Kikukawa et al., 2008), a monomeric, *mono*-aluminum-substituted α-Keggin polyoxometalate $K_6H_3[ZnW_{11}O_{40}Al]\cdot 9.5H_2O$ (Yang et al., 1997), and a dimeric aluminum complex having *mono*- and *di*-aluminum sites sandwiched by *tri*-lacunary α-Keggin polyoxometalate $K_6Na[(A\text{-}PW_9O_{34})_2\{W(OH)(OH_2)\}\{Al(OH)(OH_2)\}\{Al(\mu\text{-}OH)(OH_2)_2\}_2]\cdot 19H_2O$ (Kato et al., 2010); these structures are shown in Fig. 2.

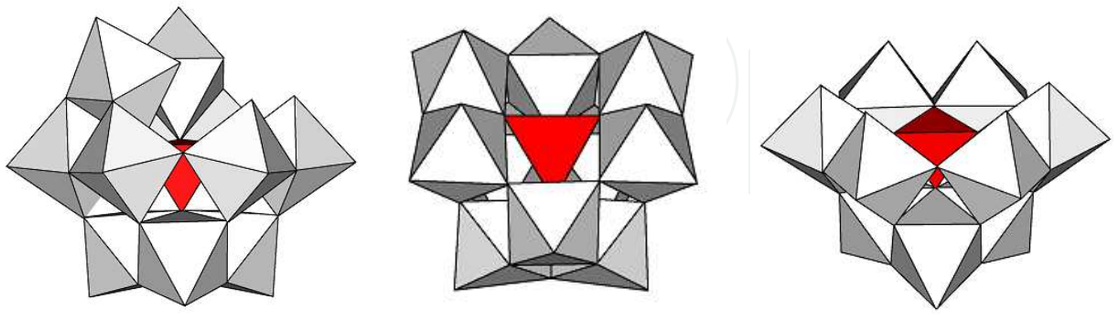

Fig. 1. Some examples of lacunary phosphotungstates. The polyhedral representations of *mono*-lacunary α-Keggin $[\alpha\text{-}PW_{11}O_{39}]^{7-}$ (left), *di*-lacunary γ-Keggin $[\gamma\text{-}PW_{10}O_{36}]^{7-}$ (center), and *tri*-lacunary α-Keggin $[A\text{-}\alpha\text{-}PW_9O_{34}]^{9-}$ (right) phosphotungstates. The WO_6 and internal PO_4 groups are represented by the white octahedra and red tetrahedron, respectively.

In this study, we successfully obtained a monomeric, α-Keggin *mono*-aluminum-substituted polyoxotungstate in the form of crystals (suitable for X-ray structure analysis) of $[(n\text{-}C_4H_9)_4N]_4[\alpha\text{-}PW_{11}\{Al(OH_2)\}O_{39}]$ that were fully characterized by X-ray crystallography; elemental analysis; thermogravimetric/differential thermal analysis; Fourier transform infrared spectroscopy; and solution ^{31}P, ^{27}Al, and ^{183}W nuclear magnetic resonance spectroscopies. Although the X-ray crystallography of $[\alpha\text{-}PW_{11}\{Al(OH_2)\}O_{39}]^{4-}$ showed that the *mono*-aluminum-substituted site was not identified because of the high symmetry in the compound, the bonding mode (bond lengths and bond angles) were significantly influenced by the insertion of aluminum ions into the *mono*-vacant sites. In addition, density-functional-theory (DFT) calculations showed a unique coordination sphere around the *mono*-aluminum-substituted site in $[\alpha\text{-}PW_{11}\{Al(OH_2)\}O_{39}]^{4-}$; this was consistent with the X-ray crystal structure and spectroscopic results. In this paper, we report the complete details of the synthesis, molecular structure, and characterization of $[(n\text{-}C_4H_9)_4N]_4[\alpha\text{-}PW_{11}\{Al(OH_2)\}O_{39}]$.

2. Experimental section

2.1 Materials

$K_7[\alpha\text{-}PW_{11}O_{39}]\cdot 11H_2O$ (Contant, 1987) and $Cs_7[\gamma\text{-}PW_{10}O_{36}]\cdot 19H_2O$ (Domaille, 1990; Knoth, 1981) were prepared as described in the literature. The number of solvated water molecules was determined by thermogravimetric/differential thermal analyses. Acetonitrile-soluble, tetra-*n*-butylammonium salts of $[\alpha\text{-}PW_{12}O_{40}]^{3-}$ and $[\alpha\text{-}PW_{11}O_{39}]^{7-}$ were prepared by the addition of excess tetra-*n*-butylammonium bromide to the aqueous solutions of $Na_3[\alpha\text{-}PW_{12}O_{40}]\cdot 16H_2O$ (Rosenheim & Jaenicke, 1917) and $K_7[\alpha\text{-}PW_{11}O_{39}]\cdot 11H_2O$. All the reagents and solvents were obtained and used as received from commercial sources. $Al(NO_3)_3\cdot 9H_2O$ (Aldrich, 99.997% purity) was used in the synthesis. The X-ray crystal structure of

$[(CH_3)_2NH_2]_4[\alpha\text{-}PW_{11}Re^{V}O_{40}]$ (Kato et al., 2010) was resolved by SHELXS-97 (direct methods) and re-refined by SHELXL-97 (Sheldrick, 2008). The crystal data are as follows: $C_8H_{32}N_3O_4PReW_{11}$: M = 3063.87, *trigonal*, space group *R-3m*, a = 16.53(2) Å, c = 25.21(4) Å, V = 5963(12) Å^3, Z = 6, D_c = 5.119 g/cm^3, R_1 = 0.0559 ($I > 2\sigma(I)$) and wR_2 = 0.1513 (for all data). The four dimethylammonium ions could not be identified due to the disorder (Nomiya et al., 2001, 2002; Weakley & Finke, 1990; Lin et al., 1993). CCDC number 851154.

2.2 Instrumentation/analytical procedures

The elemental analysis was carried out by using Mikroanalytisches Labor Pascher (Remagen, Germany). The sample was dried overnight at room temperature under pressures of 10^{-3} – 10^{-4} Torr before analysis. Infrared spectra were recorded on a Parkin Elmer Spectrum100 FT-IR spectrometer in KBr disks at room temperature. Thermogravimetric (TG) and differential thermal analyses (DTA) data were obtained using a Rigaku Thermo Plus 2 series TG/DTA TG 8120. TG/DTA measurements were performed in air by constantly increasing the temperature from 20 to 500 °C at a rate of 4 °C per min. The ^{31}P nuclear magnetic resonance (NMR) (242.95 MHz) spectra in acetonitrile-d_3 solution were recorded in tubes (outer diameter: 5 mm) on a JEOL ECA-600 NMR spectrometer. The ^{31}P NMR spectra were referenced to an external standard of 85% H_3PO_4 in a sealed capillary. Negative chemical shifts were reported on the δ scale for resonance upfields of H_3PO_4 (δ 0). The ^{27}Al NMR (156.36 MHz) spectrum in acetonitrile-d_3 was recorded in tubes (outer diameter: 5 mm) on a JEOL ECA-600 NMR spectrometer. The ^{27}Al NMR spectrum was referenced to an external standard of saturated $AlCl_3$-D_2O solution (substitution method). Chemical shifts were reported as positive on the δ scale for resonance downfields of $AlCl_3$ (δ 0). The ^{183}W NMR (25.00 MHz) spectra were recorded in tubes (outer diameter: 10 mm) on a JEOL ECA-600 NMR spectrometer. The ^{183}W NMR spectra measured in acetonitrile-d_3 were referenced to an external standard of saturated Na_2WO_4-D_2O solution (substitution method).

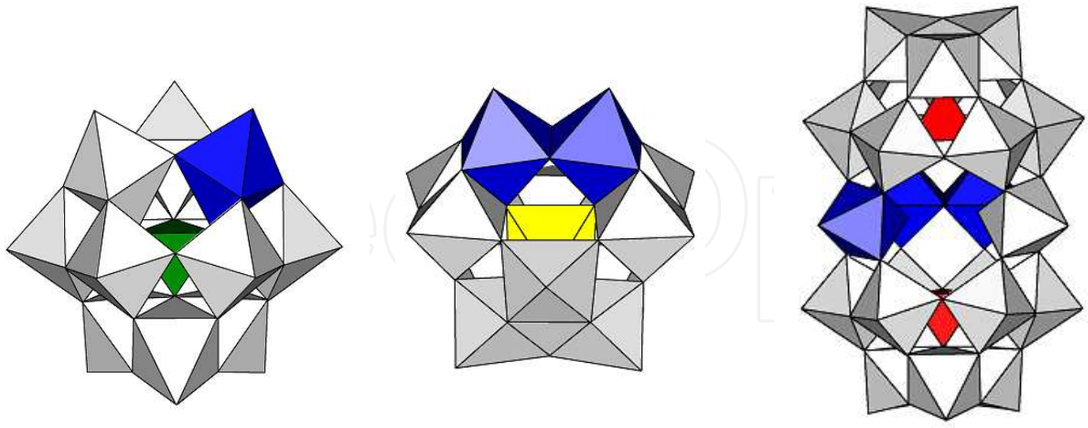

Fig. 2. The polyhedral representation of $K_6H_3[ZnW_{11}O_{40}Al]\cdot 9.5H_2O$ (left), $TBA_3H[\gamma\text{-}SiW_{10}O_{36}\{Al(OH_2)\}_2(\mu\text{-}OH)_2]\cdot 4H_2O$ (TBA = tetra-*n*-butylammonium) (center), and $K_6Na[(A\text{-}PW_9O_{34})_2\{W(OH)(OH_2)\}\{Al(OH)(OH_2)\}\{Al(\mu\text{-}OH)(OH_2)_2\}_2]\cdot 19H_2O$ (right). The aluminum groups are represented by the blue octahedra. The WO_6 groups are represented by white octahedra. The internal ZnO_4, SiO_4, and PO_4 groups are represented by green, yellow, and red tetrahedra, respectively.

Chemical shifts were reported as negative for resonance upfields of Na_2WO_4 (δ 0). Potentiometric titration was carried out with 0.4 mol/L tetra-*n*-butylammonium hydroxide as a titrant under argon atmosphere (Weiner et al., 1996). The compound $[(n\text{-}C_4H_9)_4N]_4[\alpha\text{-}PW_{11}\{Al(OH_2)\}O_{39}]$ (0.018 mmol) was dissolved in acetonitrile (30 mL) at 25 °C and the solution was stirred for approximately 5 min. The titration data were obtained with a pH meter (Mettler Toledo). Data points were obtained in milivolt. A solution of tetra-*n*-butylammonium hydroxide (9.0 mmol/L) was syringed into the suspension in 0.25-equivalent intervals.

2.3 Synthesis of $[(n\text{-}C_4H_9)_4N]_4[\alpha\text{-}PW_{11}\{Al(OH_2)\}O_{39}]$

$Cs_7[\gamma\text{-}PW_{10}O_{36}]\cdot 19H_2O$ (2.00 g; 0.538 mmol) was dissolved in water (600 mL) at 40 °C, and solid $Al(NO_3)_3\cdot 9H_2O$ (0.250 g, 0.666 mmol) was added to the colorless clear solution. After stirring for 1 h at 40 °C, a solid $[(n\text{-}C_4H_9)_4N]_4Br$ (12.14 g; 37.7 mmol) was added to the solution, followed by stirring at 25 °C for 3 days. The white precipitate was collected on a glass frit (G4) and washed with water (ca. 1 L). At this stage, a crude product was obtained in a 1.662 g yield. The crude product (1.662 g) was dissolved in acetonitrile (10 mL), followed by filtering through a folded filter paper (Whatman #5). After the product was left standing for a week at 25 °C, colorless platelet crystals were formed. The obtained crystals weighted 0.752 g (the yield calculated considering that [mol of $[(n\text{-}C_4H_9)_4N]_4[\alpha\text{-}PW_{11}\{Al(OH_2)\}O_{39}]$/[mol of $Cs_7[\gamma\text{-}PW_{10}O_{36}]\cdot 19H_2O$] × 100 was 36.9%). The elemental analysis results were as follows: C, 20.73; H, 4.00; N, 1.58; P, 0.84; Al, 0.77; W, 54.6; Cs, <0.1%. The calculated values for $[(n\text{-}C_4H_9)_4N]_4[\alpha\text{-}PW_{11}\{Al(OH_2)\}O_{39}] = C_{64}H_{146}AlN_4O_{40}PW_{11}$: C, 20.82; H, 3.99; N, 1.52; P, 0.84; Al, 0.73; W, 54.77; Cs, 0%. A weight loss of 2.16% was observed in the product during overnight drying at room temperature under 10^{-3}–10^{-4} Torr before the analysis, thereby suggesting the presence of two weakly solvated or adsorbed acetonitrile molecules (2.18%). TG/DTA under atmospheric conditions showed a weight loss of 31.0% with an exothermic peak at 337 °C was observed in the temperature range from 25 to 500 °C; our calculations indicated the presence of four $[(C_4H_9)_4N]^+$ ions, two acetonitrile molecules, and a water molecule (calcd. 28.4%). The results were as follows: IR soectroscopy results (KBr disk): 1078s, 964s, 887s, 818s, 749m, 702w, 518w cm^{-1}; ^{31}P NMR (25°C, acetonitrile-d_3): δ -12.5; ^{27}Al NMR (25 °C, acetonitrile-d_3): δ 16.1; ^{183}W NMR (25 °C, acetonitrile-d_3): δ -56.2 (2W), -93.1 (2W), -108.6 (2W), -115.8 (2W), -118.5 (1W), -153.9 (2W).

2.4 X-Ray crystallography

A colorless platelet crystal of $[(n\text{-}C_4H_9)_4N]_4[\alpha\text{-}PW_{11}\{Al(OH_2)\}O_{39}]$ (0.16 × 0.16 × 0.01 mm^3) was mounted on a MicroMount. All measurements were made on a Rigaku VariMax with a Saturn diffractometer using multi-layer mirror monochromated Mo Kα radiation (λ= 0.71075 Å) at 93 K. Data were collected and processed using CrystalClear for Windows, and structural analysis was performed using the CrystalStructure for Windows. The structure was solved by SHELXS-97 (direct methods) and refined by SHELXL-97 (Sheldrick, 2008). Since one aluminum atom was disordering over twelve tungsten sites in $[\alpha\text{-}PW_{11}\{Al(OH_2)\}O_{39}]^{4-}$, the occupancies for the aluminum and tungsten sites were fixed at 1/12 and 11/12 throughtout the refinement. Four tetra-*n*-butylammonium ions could not be modelled with disordered atoms. Accordingly, the residual electron density was removed using the SQUEEZE routine in PLATON (Spek, 2009).

2.5 Crystal data for $[(n\text{-}C_4H_9)_4N]_4[\alpha\text{-}PW_{11}\{Al(OH_2)\}O_{39}]$

$C_{64}H_{146}AlN_4O_{40}PW_{11}$; M = 3692.17, *cubic*, space group *Im-3m (#229)*, a = 17.665(2) Å, V = 5512.2(8) Å^3, Z = 2, D_c = 2.224 g/cm^3, μ(Mo-Kα) = 115.313 cm^{-1}. R_1 = 0.0220 ($I > 2\sigma(I)$) and wR_2 = 0.0554 (for all data). GOF = 1.093 (22662 total reflections, 652 unique reflections where $I > 2\sigma(I)$). CCDC number 851155.

2.6 Computational details

The optimal geometry of $[\alpha\text{-}PW_{11}\{Al(OH_2)\}O_{39}]^{4-}$ was computed by means of a DFT method. First, we optimized the crystal geometries and followed this up with single-point calculations with larger basis sets. All calculations were performed by a spin-restricted B3LYP on Gaussian09 program package (Frisch et al., 2009). The basis sets used for the geometry optimization were LANL2DZ for W atoms, 6-31+G* for P atoms and 6-31G* for H, O, and Al atoms. LANL2DZ and 6-31+G* were used for W and other atoms, respectively, for the single-point calculations. The geometry optimizations were started using the X-ray structure of $[\alpha\text{-}PW_{12}O_{40}]^{3-}$ as an initial geometry, and they were performed under the gas phase condition. The optimized geometries were confirmed to be true minima by frequency analyses. All atomic charges used in this text were obtained from Mulliken population analysis.

3. Results and discussion

3.1 Synthesis and molecular formula of $[(n\text{-}C_4H_9)_4N]_4[\alpha\text{-}PW_{11}\{Al(OH_2)\}O_{39}]$

The tetra-*n*-butylammonium salt of $[\alpha\text{-}PW_{11}\{Al(OH_2)\}O_{39}]^{4-}$ was formed by the direct reaction of aluminum nitrate with $[\gamma\text{-}PW_{10}O_{36}]^{7-}$ (the molar ratio of Al^{3+}:$[\gamma\text{-}PW_{10}O_{36}]^{7-}$ was ca. 1.0) in an aqueous solution at 40 °C under air, followed by the addition of excess tetra-*n*-butylammonium bromide. The crystallization was performed by slow-evaporation from acetonitrile at 25 °C. During the formation of $[\alpha\text{-}PW_{11}\{Al(OH_2)\}O_{39}]^{4-}$, the decomposition of a *di*-lacunary γ-Keggin polyoxotungstate, and isomerization of γ-isomer to α-isomer occurred in order to construct the *mono*-aluminum-substituted site in an α-Keggin structure. It was noted that the polyoxoanion $[\alpha\text{-}PW_{11}\{Al(OH_2)\}O_{39}]^{4-}$ was easily obtained by the stoichiometric reaction of aluminum nitrate with a *mono*-lacunary α-Keggin polyoxotungstate, $[\alpha\text{-}PW_{11}O_{39}]^{7-}$, in an aqueous solution; however, a single species of $[\alpha\text{-}PW_{11}\{Al(OH_2)\}O_{39}]^{4-}$ could not be obtained as a tetra-*n*-butylammonium salt by using $[\alpha\text{-}PW_{11}O_{39}]^{7-}$ as a starting polyoxoanion.[1] Thus, single crystals that were suitable for X-ray crystallography could be obtained for the crystallization of the tetra-*n*-butylammonium salt of $[\alpha\text{-}PW_{11}\{Al(OH_2)\}O_{39}]^{4-}$ synthesized by using a *di*-lacunary γ-Keggin polyoxotungstate.

[1] The ^{31}P NMR spectrum in acetonitrile-d_3 of the tetra-*n*-butylammonium salt of $[\alpha\text{-}PW_{11}\{Al(OH_2)\}O_{39}]^{4-}$ prepared by the stoichiometic reaction of $[\alpha\text{-}PW_{11}O_{39}]^{7-}$ with $Al(NO_3)_3{\cdot}9H_2O$ in an aqueous solution showed two signals at -12.35 ppm and -12.48 ppm. The signal at -12.48 ppm was assigned to the internal phosphorus atom in $[\alpha\text{-}PW_{11}\{Al(OH_2)\}O_{39}]^{4-}$, whereas the signal at -12.35 ppm could not be identified; however, the signal was not due to the proton isomer, as reported for $[(CH_3)_2NH_2]_{10}[Hf(PW_{11}O_{39})_2]{\cdot}8H_2O$ (Hou et al., 2007).

The sample for the elemental analysis was dried overnight at room temperature under a vacuum of 10^{-3} – 10^{-4} Torr. The elemental results for C, H, N, P, Al, and W were in good agreement with the calculated values for the formula without any absorbed or solvated molecules for $[(n\text{-}C_4H_9)_4N]_4[\alpha\text{-}PW_{11}\{Al(OH_2)\}O_{39}]$.

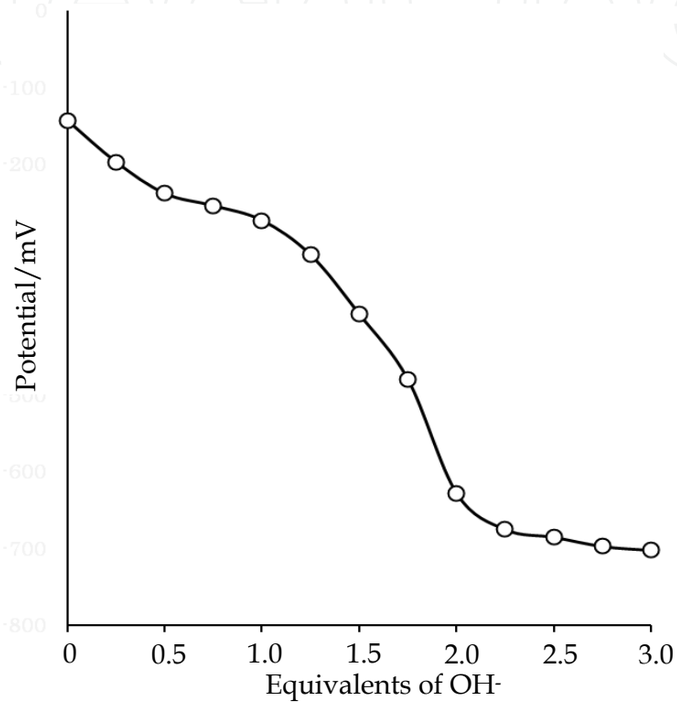

Fig. 3. Profile for the potentiometric titration of $[(n\text{-}C_4H_9)_4N]_4[\alpha\text{-}PW_{11}\{Al(OH_2)\}O_{39}]$ with tetra-*n*-butylammonium hydroxide as a titrant.

The Cs analysis revealed no contamination of cesium ions from $Cs_7[\gamma\text{-}PW_{10}O_{36}]\cdot 19H_2O$. The weight loss observed during the course of drying before the analysis was 2.16% for $[(n\text{-}C_4H_9)_4N]_4[\alpha\text{-}PW_{11}\{Al(OH_2)\}O_{39}]$; this corresponded to two weakly solvated or adsorbed acetonitrile molecules. On the other hand, in the TG/DTA measurement performed under atmospheric conditions, a weight loss of 31.0% observed in the temperature range from 25 to 500 °C corresponded to four tetra-*n*-butylammonium ions, two acetonitrile molecules, and a water molecule.

From the potentiometric titration, a break point at 2.0 equivalents of added base was observed, as shown in Fig. 3. The titration profile revealed that $[(n\text{-}C_4H_9)_4N]_4[\alpha\text{-}PW_{11}\{Al(OH_2)\}O_{39}]$ had two titratable protons dissociated from the Al-OH_2 group. This result was consistent with the elemental analysis result.

3.2 The molecular structure of $[(n\text{-}C_4H_9)_4N]_4[\alpha\text{-}PW_{11}\{Al(OH_2)\}O_{39}]$

The molecular structure of $[\alpha\text{-}PW_{11}\{Al(OH_2)\}O_{39}]^{4-}$ as determined by X-ray crystallography is shown in Figs. 4 and 5. The bond lengths and bond angles are summarized in appendix. The molecular structure of $[\alpha\text{-}PW_{11}\{Al(OH_2)\}O_{39}]^{4-}$ was identical to that of a monomeric, α-Keggin polyoxotungstate $[\alpha\text{-}PW_{12}O_{40}]^{3-}$ (Neiwert et al., 2002; Busbongthong & Ozeki, 2009). Due to the high symmetry space group, the eleven tungsten(VI) atoms were disordered and the *mono*-aluminum-substituted site was not identified, as observed for $[W_9ReO_{32}]^{5-}$ (Ortéga et al., 1997), $[\alpha\text{-}PW_{11}Re^{V}O_{40}]^{5-}$ (Kato et al., 2010), $[\{SiW_{11}O_{39}Cu(H_2O)\}\{Cu_2(ac)\text{-}(phen)_2(H_2O)\}]^{14-}$ (phen = phenanthroline, ac = acetate) (Reinoso et al., 2006), $(ANIH)_5[PCu(H_2O)W_{11}O_{39}](ANI)\cdot 8H_2O$ (ANI = aniline, $ANIH^+$ = anilinium ion) (Fukaya et al., 2011), $Cs_5[PMn(H_2O)W_{11}O_{39}]\cdot 4H_2O$ (Patel et al., 2011), and $Cs_5[PNi(H_2O)W_{11}O_{39}]\cdot 2H_2O$ (T. J. R. Weakley, 1987). However, the bond lengths of $[(n\text{-}C_4H_9)_4N]_4[\alpha\text{-}PW_{11}\{Al(OH_2)\}O_{39}]$ were clearly influenced by the insertion of aluminum ion into the vacant site as compared with those of $[CH_3NH_3]_3[PW_{12}O_{40}]\cdot 2H_2O$, $[(CH_3)_2NH_2]_3[PW_{12}O_{40}]$, and $[(CH_3)_3NH]_3\text{-}[PW_{12}O_{40}]$ (Busbongthong & Ozeki, 2009) (Table 1). Thus, the lengths of the oxygen atoms belonging to the central PO_4 tetrahedron (O_a) are longer than those of the three alkylammonium salts of $[PW_{12}O_{40}]^{3-}$; whereas, the lengths of the bridging oxygen atoms between corner-sharing MO_6 (M = W and Al) octahedra (O_c) and bridging oxygen atoms between edge-sharing MO_6 octahedra (O_e) are shorter than those of $[PW_{12}O_{40}]^{3-}$. For comparisons, the bond lengths of *mono*-metal-substituted α-Keggin phosphotungstates, e.g., $[(CH_3)_2NH_2]_4[\alpha\text{-}PW_{11}Re^{V}O_{40}]$, $(ANIH)_5[PCu(H_2O)W_{11}O_{39}](ANI)\cdot 8H_2O$ (ANI = aniline,

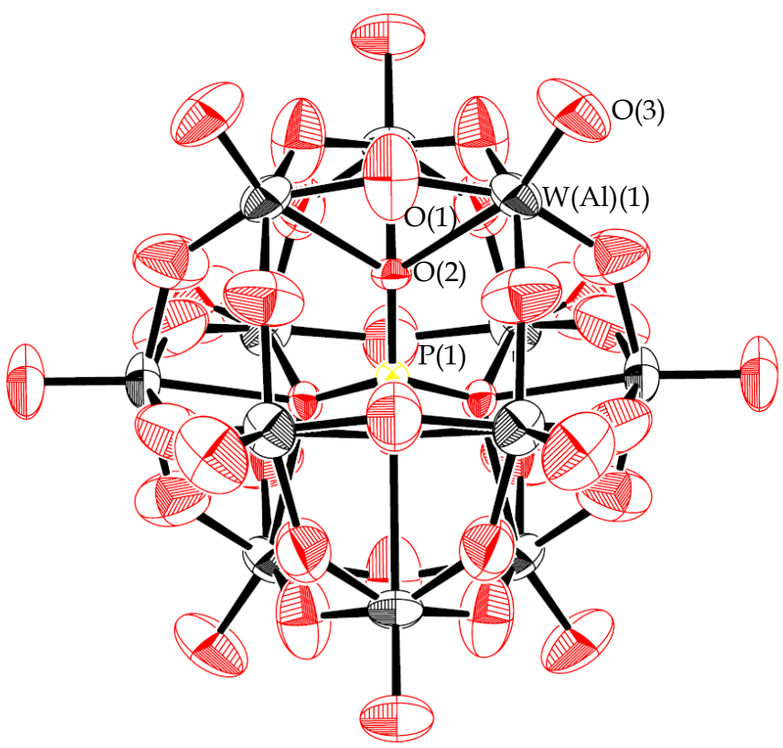

Fig. 4. The molecular structure (ORTEP drawing) of $[\alpha\text{-}PW_{11}\{Al(OH_2)\}O_{39}]^{4-}$.

	$[(n\text{-}C_4H_9)_4N]_4[\alpha\text{-}PW_{11}\{Al(OH_2)\}O_{39}]$
W(Al)-O_a	2.466 (2.466)
W(Al)-O_c	1.883 (1.883)
W(Al)-O_e	1.883 (1.883)
W(Al)-O_t	1.667 (1.667)
P-O	1.5206 (1.5206)
	$[CH_3NH_3]_3[\alpha\text{-}PW_{12}O_{40}]\cdot 2H_2O$
W-O_a	2.4077 - 2.4606 (2.4398)
W-O_c	1.8766 - 1.9407 (1.9076)
W-O_e	1.8808 - 1.9448 (1.9166)
W-O_t	1.6818 - 1.7068 (1.6951)
P-O	1.5286 - 1.5377 (1.5324)
	$[(CH_3)_2NH_2]_3[\alpha\text{-}PW_{12}O_{40}]$
W-O_a	2.4273 - 2.4568 (2.4430)
W-O_c	1.9044 - 1.9164 (1.9103)
W-O_e	1.9029 - 1.9234 (1.9158)
W-O_t	1.7000 - 1.7038 (1.7026)
P-O	1.5220 - 1.5348 (1.5313)
	$[(CH_3)_3NH]_3[\alpha\text{-}PW_{12}O_{40}]$
W-O_a	2.4313 – 2.4497 (2.4313)
W-O_c	1.8840 – 1.9286 (1.9127)
W-O_e	1.8996 – 1.9437 (1.9186)
W-O_t	1.6890 - 1.6970 (1.6933)
P-O	1.5296 – 1.5355 (1.5340)

Table 1. Ranges and mean bond distances (Å) for $[(n\text{-}C_4H_9)_4N]_4[\alpha\text{-}PW_{11}\{Al(OH_2)\}O_{39}]$, and the three alkylammonium salts of $[PW_{12}O_{40}]^{3-}$. The terms O_a, O_c, O_e, and O_t are explained in Fig. 5. The mean values are provided in parentheses.

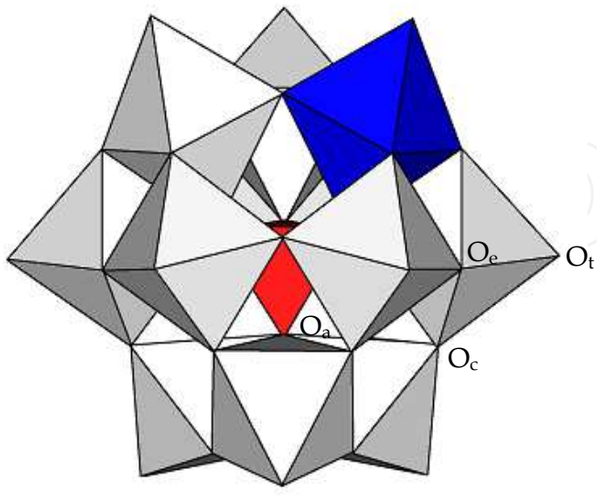

Fig. 5. The polyhedral representation of $[\alpha\text{-}PW_{11}\{Al(OH_2)\}O_{39}]^{4-}$. In the polyhedral representation, the AlO_6 and WO_6 groups are represented by blue and white octahedra, respectively. The internal PO_4 group is represented by the red tetrahedron. Further, O_a,

oxygen atoms belonging to the central PO_4 tetrahedron; O_c, bridging oxygen atoms between corner-sharing MO_6 (M = Al and W) octahedra; O_e, bridging oxygen atoms between edge-sharing MO_6 octahedra (M = Al and W); O_t, terminal oxygen atoms.

$ANIH^+$ = anilinium ion), $Cs_5[PMn(H_2O)W_{11}O_{39}]\cdot 4H_2O$, and $Cs_5[PNi(H_2O)W_{11}O_{39}]\cdot 2H_2O$ as determined by X-ray crystallography are summarized in Table 2. Although a simple comparison was difficult to draw, the following trends were observed: The W-O_a bond lengths of $[PCu(H_2O)W_{11}O_{39}]^{5-}$, $[PMn(H_2O)W_{11}O_{39}]^{5-}$, and $[PNi(H_2O)W_{11}O_{39}]^{5-}$ were significantly longer than those of $[\alpha\text{-}PW_{12}O_{40}]^{3-}$ and $[\alpha\text{-}PW_{11}Re^{V}O_{40}]^{4-}$, as observed for $[\alpha\text{-}PW_{11}\{Al(OH_2)\}O_{39}]^{4-}$ due to the presence of a water molecule coordinated to the *mono*-metal-substituted sites. The W(M)-O_c and W(M)-O_e (M = Re, Cu, Mn, and Ni) bond lengths of the four polyoxoanions mentioned in Table 2 were similar to those of $[\alpha\text{-}PW_{12}O_{40}]^{3-}$, whereas, the bond lengths of $[\alpha\text{-}PW_{11}\{Al(OH_2)\}O_{39}]^{4-}$ were clearly shorter than those of $[\alpha\text{-}PW_{12}O_{40}]^{3-}$.

	$[(CH_3)_2NH_2]_4[\alpha\text{-}PW_{11}Re^{V}O_{40}]$
W(Re)-O_a	2.418 – 2.441 (2.432)
W(Re)-O_c	1.896 – 1.914 (1.906)
W(Re)-O_e	1.895 – 1.922 (1.907)
W(Re)-O_t	1.647 – 1.694 (1.680)
P-O	1.538 – 1.540 (1.539)
	$(ANIH)_5[PCu(H_2O)W_{11}O_{39}](ANI)\cdot 8H_2O$
W(Cu)-O_a	2.4784 - 2.5044 (2.4916)
W(Cu)-O_c	1.8946 - 1.9277 (1.9077)
W(Cu)-O_e	1.8946 - 1.9277 (1.9077)
W(Cu)-O_t	1.7163 - 1.7220 (1.7178)
P-O	1.4925 - 1.5078 (1.4965)
	$Cs_5[PMn(H_2O)W_{11}O_{39}]\cdot 4H_2O$
W(Mn)-O_a	2.4220 - 2.5520 (2.4874)
W(Mn)-O_c	1.9223 - 1.8698(1.9051)
W(Mn)-O_e	1.8689 - 1.9620 (1.9079)
W(Mn)-O_t	1.6678 - 1.752(1.6889)
P-O	1.4902 - 1.602 (1.5265)
	$Cs_5[PNi(H_2O)W_{11}O_{39}]\cdot 2H_2O$
W(Ni)-O_a	2.4013 - 2.5152 (2.4792)
W(Ni)-O_c	1.8628 - 1.9430 (1.8974)
W(Ni)-O_e	1.8633 - 1.9421 (1.8964)
W(Ni)-O_t	1.6714 - 1.7354 (1.7010)
P-O	1.5150 - 1.5256 (1.5209)

Table 2. Ranges and mean bond distances (Å) for four *mono*-metal-substituted α-Keggin phosphotungstates. The terms O_a and O_t are explained in Fig. 5. The terms O_c and O_e indicate bridging oxygen atoms between corner- and edge-sharing MO_6 (M = W, Re, Cu, Mn, Ni) octahedra. The mean values are provided in parentheses.

To investigate the coordination sphere around the *mono*-aluminum-substituted site in $[\alpha\text{-}PW_{11}\{Al(OH_2)\}O_{39}]^{4-}$, the optimized geometry was computed by means of a DFT method, as

shown in Figs. 6 and 7. The ranges and mean bond distances, and the Millken charges for the DFT-optimized $[\alpha\text{-}PW_{11}\{Al(OH_2)\}O_{39}]^{4-}$ are summarized in Tables 3 and 4. It was noted that the *mono*-aluminum-substituted site was uniquely concave downward, which caused the extension of the P-O bond linkaged to the aluminum atom (1.5654 Å), whereas the Al-O bond linkaged to the internal phosphorus atom was shortened due to the insertion of the Al^{3+} ion that has a smaller ionic radius (0.675 Å) than that of W^{6+} (0.74 Å) into the *mono*-vacant site (Shannon, 1976). The lengths of Al-O bonds at the corner- and edge-sharing Al-O-W bondings were shorter than those of W-O bonds at the corner- and edge-sharing W-O-W bondings, which caused shortening of the average W(Al)-O bond lengths, as observed by X-ray crystallography.

The Mulliken charges of all oxygen atoms linkaged to aluminum atoms in $[\alpha\text{-}PW_{11}\{Al(OH_2)\}O_{39}]^{4-}$ were more positive than those linkaged to tungsten atoms in $[\alpha\text{-}PW_{12}O_{40}]^{3-}$; whereas the charges of oxygen atoms linkaged to tungsten atoms in $[\alpha\text{-}PW_{11}\{Al(OH_2)\}O_{39}]^{4-}$ were similar to those in $[\alpha\text{-}PW_{12}O_{40}]^{3-}$. In addition, the atomic charge of the phosphorus atom in $[\alpha\text{-}PW_{11}\{Al(OH_2)\}O_{39}]^{4-}$ was more negative than that in $[\alpha\text{-}PW_{12}O_{40}]^{3-}$. In the case of *mono*-vanadium(V)-substituted Keggin silicotungstate $[SiW_{11}VO_{40}]^{5-}$, the net charge associated with the inner tetrahedron was very similar to that supported by SiO_4 in $[SiW_{12}O_{40}]^{4-}$ (Maestre et al., 2001). Thus, the difference in the charge on the internal phosphorus atom for $[\alpha\text{-}PW_{11}\{Al(OH_2)\}O_{39}]^{4-}$ and $[\alpha\text{-}PW_{12}O_{40}]^{3-}$ might be due to the gravitation of aluminum atoms towards the internal PO_4 group.

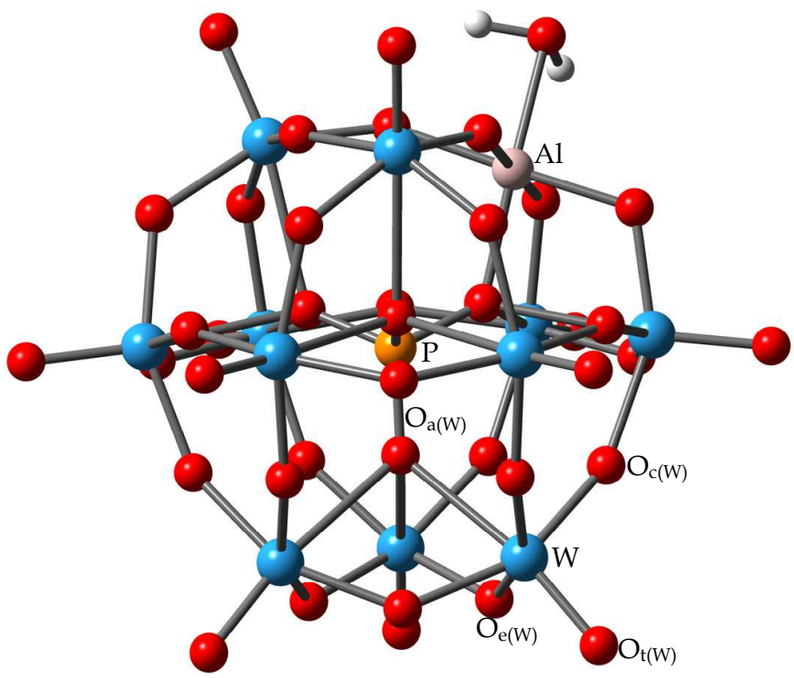

Fig. 6. The DFT-optimized geometry of $[\alpha\text{-}PW_{11}\{Al(OH_2)\}O_{39}]^{4-}$. The phosphorus, oxygen, aluminum, tungsten, and hydrogen atoms are represented by orange, red, pink, blue, and white balls, respectively.

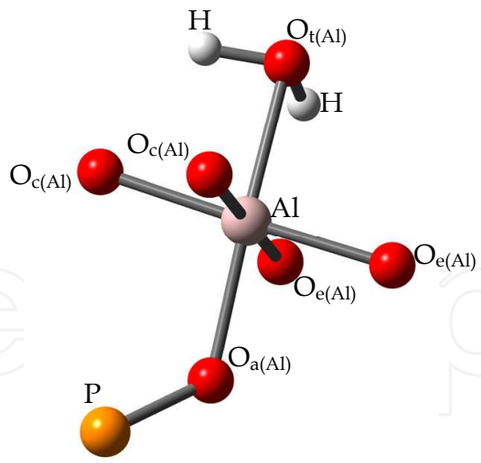

Fig. 7. The coordination sphere around the *mono*-aluminum-substituted site in DFT-optimized $[\alpha\text{-}PW_{11}\{Al(OH_2)\}O_{39}]^{4-}$.

	$[\alpha\text{-}PW_{11}\{Al(OH_2)\}O_{39}]^{4-}$	$[\alpha\text{-}PW_{12}O_{40}]^{3-}$
W-O_a	2.4422 – 2.5140 (2.4702)	2.4568 – 2.4579 (2.4574)
W-O_c	1.8311 – 1.9828 (1.9206)	1.9202 – 1.9216 (1.9209)
W-O_e	1.8373 – 1.9918 (1.9267)	1.9262 – 1.9276 (1.9267)
W-O_t	1.7196 – 1.7246 (1.7210)	1.7103 – 1.7106 (1.7105)
P-O	1.5450 – 1.5654 (1.5517)	1.5530 – 1.5535 (1.5533)
Al-O_a	1.9487 (1.9487)	–
Al-O_c	1.8519, 1.8955 (1.8737)	–
Al-O_e	1.8723, 1.9215 (1.8969)	–
Al-OH_2	2.0983 (2.0983)	–

Table 3. Ranges and mean bond distances (Å) for $[\alpha\text{-}PW_{11}\{Al(OH_2)\}O_{39}]^{4-}$ and $[\alpha\text{-}PW_{12}O_{40}]^{3-}$ optimized by DFT calculations. The terms O_a, O_c, O_e, and O_t are explained in Fig. 5. The average values are provided in parentheses.

	$[\alpha\text{-}PW_{11}\{Al(OH_2)\}O_{39}]^{4-}$	$[\alpha\text{-}PW_{12}O_{40}]^{3-}$
$O_{a\,(W)}$	-0.7356 – -0.8445 (-0.7734)	-0.8951 – -0.8990 (-0.8968)
$O_{c\,(W)}$	-1.226 – -1.345 (-1.317)	-1.353 – -1.355 (-1.353)
$O_{e\,(W)}$	-1.030 – -1.160 (-1.074)	-1.085 – -1.087 (-1.086)
$O_{t\,(W)}$	-0.6757 – -0.6991 (-0.6882)	-0.6273 – -0.6277 (-0.6275)
P	7.255 (7.255)	9.256 (9.256)
W	2.101 – 2.343 (2.257)	2.343 – 2.346 (2.345)
$O_{a(Al)}$	-0.1495 (-0.1495)	-
$O_{c(Al)}$	-0.3332, -0.5920 (-0.4626)	-
$O_{e(Al)}$	-0.4910, -0.7848 (-0.6379)	-
$O_{t(Al)}$	-0.5553 (-0.5553)	-
Al	-0.5307 (-0.5307)	-
H	0.5754, 0.5796 (0.5775)	-

Table 4. Mulliken charges computed for $[\alpha\text{-}PW_{11}\{Al(OH_2)\}O_{39}]^{4-}$ and $[\alpha\text{-}PW_{12}O_{40}]^{3-}$. The terms $O_{a(M)}$, $O_{c(M)}$, $O_{e(M)}$, and $O_{t(M)}$ (M = Al and W) are explained in Figs. 6 and 7. The average values are provided in parentheses.

3.2 Spectroscopic data for $[(n\text{-}C_4H_9)_4N]_4[\alpha\text{-}PW_{11}\{Al(OH_2)\}O_{39}]$

The FTIR spectra measured as a KBr disk of $[(n\text{-}C_4H_9)_4N]_4[\alpha\text{-}PW_{11}\{Al(OH_2)\}O_{39}]$, $K_7[\alpha\text{-}PW_{11}O_{39}]\cdot 11H_2O$, $Cs_7[\gamma\text{-}PW_{10}O_{36}]\cdot 19H_2O$, and $Na_3[\alpha\text{-}PW_{12}O_{40}]\cdot 16H_2O$ are shown in Fig. 8. For

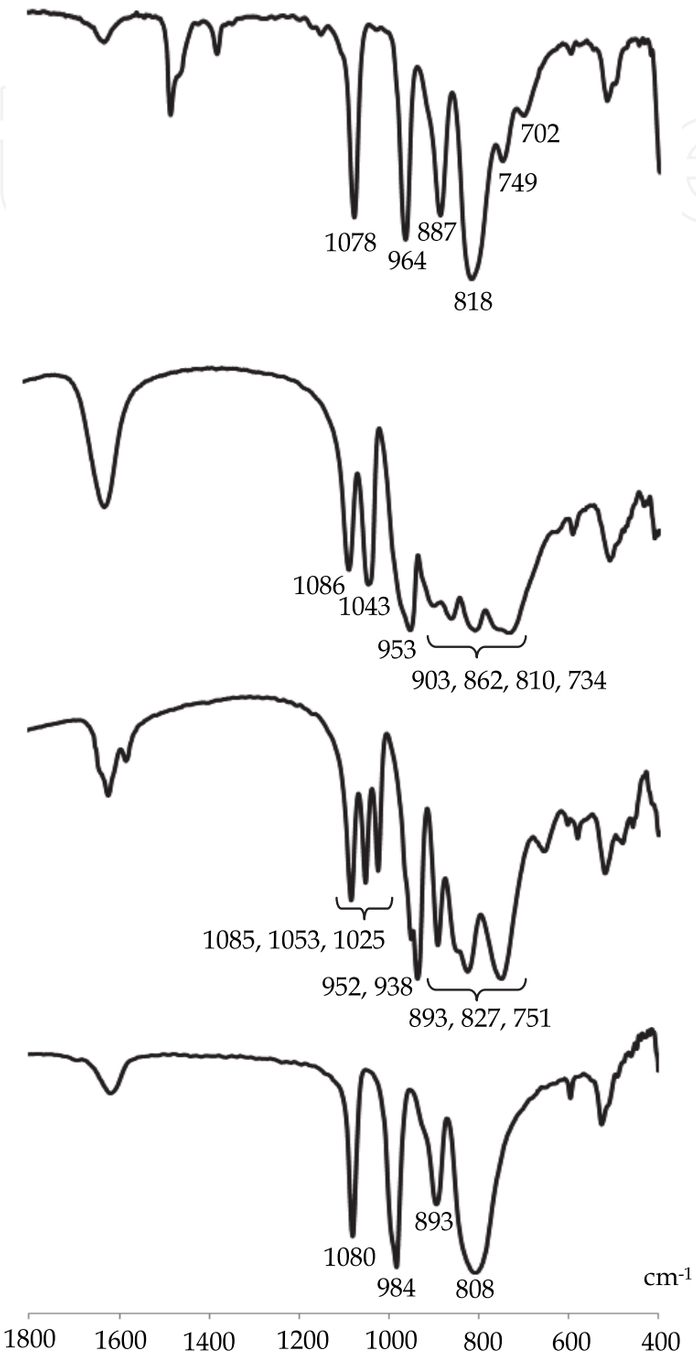

Fig. 8. FTIR spectra (as KBr disks) in the range of 1800 – 400 cm^{-1} for $[(n\text{-}C_4H_9)_4N]_4[\alpha\text{-}PW_{11}\{Al(OH_2)\}O_{39}]$ (top), $K_7[\alpha\text{-}PW_{11}O_{39}]\cdot 11H_2O$ (the second top), $Cs_7[\gamma\text{-}PW_{10}O_{36}]\cdot 19H_2O$ (the third top), and $Na_3[\alpha\text{-}PW_{12}O_{40}]\cdot 16H_2O$ (bottom)

$[(n\text{-}C_4H_9)_4N]_4[\alpha\text{-}PW_{11}\{Al(OH_2)\}O_{39}]$, the P-O band was observed at 1078 cm^{-1}, and the W-O bands were observed at 964, 887, 818, 749, and 702 cm^{-1}, these were different from those of $K_7[\alpha\text{-}PW_{11}O_{39}]\cdot 11H_2O$ (1086, 1043, 953, 903, 862, 810, and 734 cm^{-1}) and $Cs_7[\gamma\text{-}PW_{10}O_{36}]\cdot 19H_2O$ (1085, 1053, 1025, 952, 938, 893, 827, and 751 cm^{-1}) (Rocchiccioli-Deltcheff et al., 1983; Thouvenot et al., 1984). This result suggested that the aluminum atom was coordinated into the vacant site in the polyoxometalate. It should be noted that the bands observed for $[(n\text{-}C_4H_9)_4N]_4[\alpha\text{-}PW_{11}\{Al(OH_2)\}O_{39}]$ were significantly different from those of $Na_3[\alpha\text{-}PW_{12}O_{40}]\cdot 16H_2O$ (1080, 984, 893, and 808 cm^{-1}). This was consistent with the results observed by X-ray crystallography and DFT calculations, as mentioned above.

The ^{31}P NMR spectrum of $[(n\text{-}C_4H_9)_4N]_4[\alpha\text{-}PW_{11}\{Al(OH_2)\}O_{39}]$ in acetonitrile-d_3 at ~25 °C was a clear single line spectrum at -12.5 ppm due to the internal phosphorus atom, thereby confirming the compound's purity and homogeneity, as shown in Fig. 9. The signal exhibited a shift from the signals of tetra-*n*-butylammonium salts of $[\alpha\text{-}PW_{12}O_{40}]^{3-}$ (δ -14.6) and $[\alpha\text{-}PW_{11}O_{39}]^{7-}$ (δ -12.0), suggesting the insertion of aluminum ion into the vacant site.

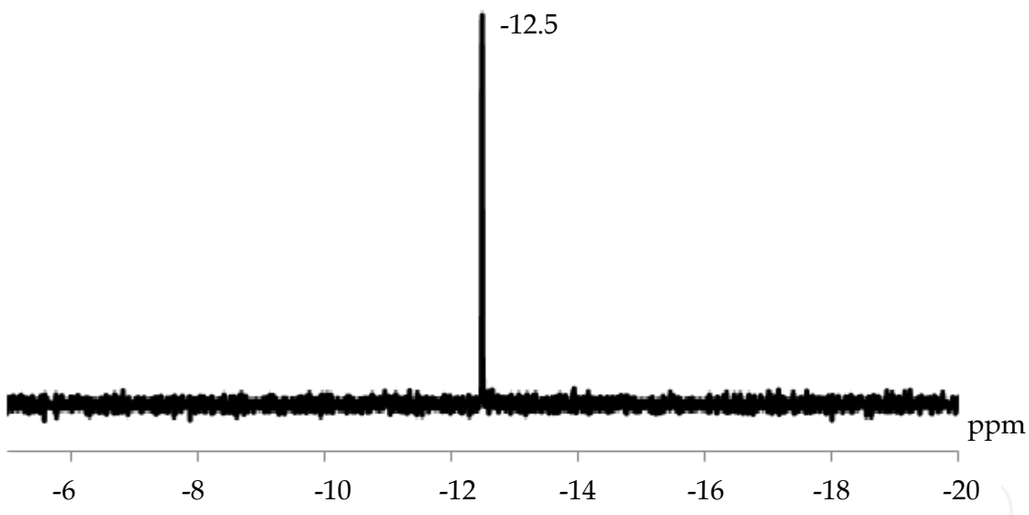

Fig. 9. ^{31}P NMR spectrum in acetonitrile-d_3 of $[(n\text{-}C_4H_9)_4N]_4[\alpha\text{-}PW_{11}\{Al(OH_2)\}O_{39}]$.

The ^{27}Al NMR spectrum (Fig. 10) of $[(n\text{-}C_4H_9)_4N]_4[\alpha\text{-}PW_{11}\{Al(OH_2)\}O_{39}]$ in acetonitrile-d_3 at ~25 °C showed a broad signal at 16.1 ppm due to the *mono*-aluminum-substituted site in $[\alpha\text{-}PW_{11}\{Al(OH_2)\}O_{39}]^{4-}$.

The ^{183}W NMR spectrum (Fig. 11) of $[(n\text{-}C_4H_9)_4N]_4[\alpha\text{-}PW_{11}\{Al(OH_2)\}O_{39}]$ in acetonitrile-d_3 at ~25 °C was a six-line spectrum of (δ -56.2, -93.1, -108.6, -115.8, -118.5, -153.9) with 2:2:2:2:1:2 intensities, which were in accordance with the presence of eleven tungsten atoms with *Cs* symmetry. These spectral data were completely consistent with the X-ray structure and the optimized structure, suggesting that the solid structure was maintained in the solution.

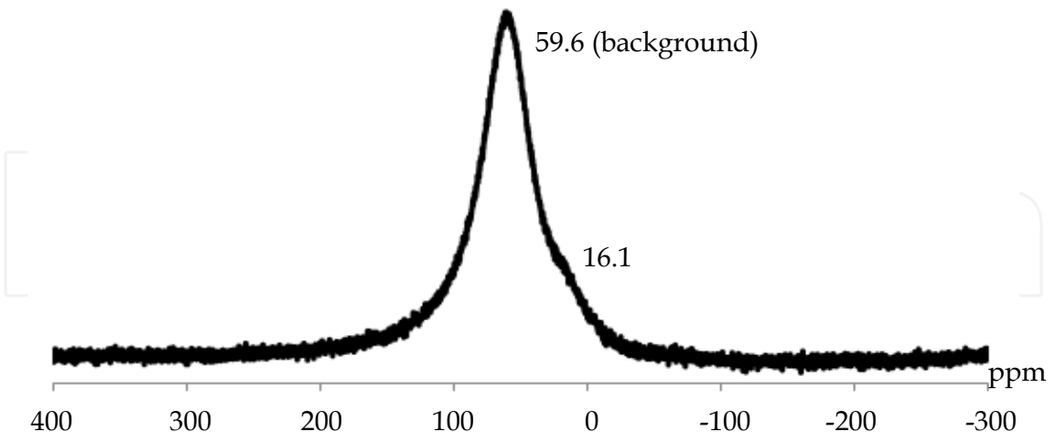

Fig. 10. ^{27}Al NMR spectrum in acetonitrile-d_3 of $[(n\text{-}C_4H_9)_4N]_4[\alpha\text{-}PW_{11}\{Al(OH_2)\}O_{39}]$.

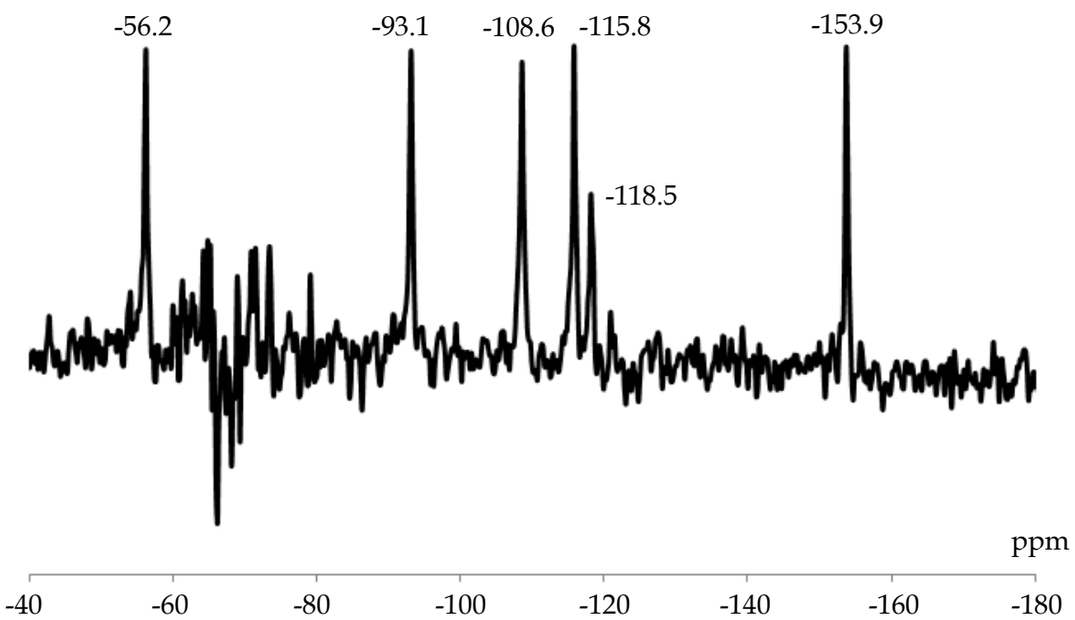

Fig. 11. ^{183}W NMR spectrum in acetonitrile-d_3 of $[(n\text{-}C_4H_9)_4N]_4[\alpha\text{-}PW_{11}\{Al(OH_2)\}O_{39}]$.

4. Conclusion

The synthesis of a monomeric, *mono*-aluminum-substituted α-Keggin polyoxometalate is described in this study. We successfully obtained single crystals of acetonitrile-soluble tetra-*n*-butylammonium salt $[(n\text{-}C_4H_9)_4N]_4[\alpha\text{-}PW_{11}\{Al(OH_2)\}O_{39}]$ by reacting aluminum nitrate with a *di*-lacunary γ-Keggin phosphotungstate. The characterization of $[(n\text{-}C_4H_9)_4N]_4[\alpha\text{-}PW_{11}\{Al(OH_2)\}O_{39}]$ was accomplished by X-ray crystallography, elemental analysis,

thermogravimetric/differential thermal analysis, Fourier transform infrared spectra, and solution ^{31}P, ^{27}Al, and ^{183}W nuclear magnetic resonance spectroscopy. The single-crystal X-ray structure analysis, revealed as $[(n\text{-}C_4H_9)_4N]_4[\alpha\text{-}PW_{11}\{Al(OH_2)\}O_{39}]$, was a monomeric, α-Keggin structure, and the *mono*-aluminum-substituted site could not be identified due to the high symmetry in the product. In contrast, the DFT-optimized geometry of $[\alpha\text{-}PW_{11}\{Al(OH_2)\}O_{39}]^{4-}$ showed that the *mono*-aluminum-substituted site was uniquely concave downward, which caused the extension of the P-O bond linkaged to the aluminum atom, whereas the Al-O bond linkaged to the phosphorus atom was shortened. This structural difference strongly influenced the bonding mode (bond lengths and bond angles) as determined by X-ray crystallography. In addition, the Mulliken charges clearly exhibited the effect caused by the insertion of aluminum atoms into the *mono*-vacant sites.

5. Acknowledgment

This work was supported by a Grant-in-Aid for Scientific Research on Innovative Areas (No. 21200055) of the Ministry of Education, Culture, Sports, Science and Technology, Japan. Y. Kataoka acknowledges the JSPS Research Fellowship for Young Scientist. Y. Kitagawa also has been supported by Grant-in-Aid for Scientific Research on Innovative Areas ("Coordination Programming" area 2170, No. 22108515) from the Ministry of Education, Culture, Sports, Science and Technology (MEXT). This research was partially carried out using equipment at the Center for Instrumental Analysis, Shizuoka University.

6. Appendix

Bond lengths (Å) of $[(n\text{-}C_4H_9)_4N]_4[\alpha\text{-}PW_{11}\{Al(OH_2)\}O_{39}]$: W(1)-O(1) 1.883(4); W(1)-O(1)^1 1.883(4); W(1)-O(1)^2 1.883(4); W(1)-O(1)^3 1.883(4); W(1)-O(2) 2.465(5); W(1)-O(2)^4 2.465(5); W(1)-O(3) 1.667(4); P(1)-O(2) 1.522(5); P(1)-O(2)^5 1.522(5); P(1)-O(2)^6 1.522(5); P(1)-O(2)^7 1.522(5); P(1)-O(2)^4 1.522(5); P(1)-O(2)^8 1.522(5); P(1)-O(2)^9 1.522(5); P(1)-O(2)^{10} 1.522(5); Al(1)-O(1) 1.883(4); Al(1)-O(1)^1 1.883(4); Al(1)-O(1)^2 1.883(4); Al(1)-O(1)^3 1.883(4); Al(1)-O(3) 1.667(4). Symmetry operators: (1) X,Z,Y (2) Z,Y,-X+1 (3) Z,-X+1,Y (4) Y,Z,-X+1 (5) Y,Z,X (6) Z,X,Y (7) X,Y,-Z+1 (8) Z,X,-Y+1 (9) -Z+1,X,-Y+1 (10) -Y+1,-Z+1,-X+1.

Bond angles (°) of $[(n\text{-}C_4H_9)_4N]_4[\alpha\text{-}PW_{11}\{Al(OH_2)\}O_{39}]$: O(1)-W(1)-O(1)^1 87.5(2); O(1)-W(1)-O(1)^2 87.08(18); O(1)-W(1)-O(1)^3 154.8(2); O(1)-W(1)-O(2) 63.32(19); O(1)-W(1)-O(2)^4 92.40(18); O(1)-W(1)-O(3) 102.58(17); O(1)^1-W(1)-O(1)^2 154.8(2) O(1)^1-W(1)-O(1)^3 87.08(18); O(1)^1-W(1)-O(2) 63.32(19); O(1)^1-W(1)-O(2)^4 92.40(18); O(1)^1-W(1)-O(3) 102.58(17); O(1)^2-W(1)-O(1)^3 87.5(2); O(1)^2-W(1)-O(2) 92.40(18); O(1)^2-W(1)-O(2)^4 63.32(19); O(1)^2-W(1)-O(3) 102.58(17); O(1)^3-W(1)-O(2) 92.40(18); O(1)^3-W(1)-O(2)^4 63.32(19); O(1)^3-W(1)-O(3) 102.58(17); O(2)-W(1)-O(2)^4 41.76(15); O(2)-W(1)-O(3) 159.12(11); O(2)^4-W(1)-O(3) 159.12(11); O(2)-P(1)-O(2)^5 109.5(3); O(2)-P(1)-O(2)^6 109.5(3); O(2)-P(1)-O(2)^7 70.5(3); O(2)-P(1)-O(2)^4 70.5(3); O(2)-P(1)-O(2)^8 180.0(4); O(2)-P(1)-O(2)^9 109.5(3); O(2)-P(1)-O(2)^{10} 70.5(3); O(2)^5-P(1)-O(2)^6 109.5(3); O(2)^5-P(1)-O(2)^7 70.5(3); O(2)^5-P(1)- O(2)^4 70.5(3); O(2)^5-P(1)-O(2)^8 70.5(3); O(2)^5-P(1)-O(2)^9 109.5(3); O(2)^5-P(1)-O(2)^{10} 180.0(4); O(2)^6-P(1)-O(2)^7 180.0(4); O(2)^6-P(1)-O(2)^4 70.5(3); O(2)^6-P(1)-O(2)^8 70.5(3); O(2)^6-P(1)-O(2)^9 109.5(3); O(2)^6-P(1)-O(2)^{10} 70.5(3); O(2)^7-P(1)-O(2)^4 109.5(3); O(2)^7-P(1)-O(2)^8 109.5(3); O(2)^7-P(1)-O(2)^9 70.5(3); O(2)^7-P(1)-O(2)^{10} 109.5(3); O(2)^4-P(1)-O(2)^8 109.5(3); O(2)^4-P(1)-O(2)^9 180.0(4); O(2)^4-P(1)-O(2)^{10} 109.5(3); O(2)^8-P(1)-O(2)^9 70.5(3); O(2)^8-P(1)-O(2)^{10} 109.5(3); O(2)^9-P(1)-O(2)^{10} 70.5(3); O(1)-Al(1)-O(1)^1 87.5(2); O(1)-

Al(1)-O(1)^{2} 87.08(18); O(1)-Al(1)–O(1)^{3} 154.8(2); O(1)-Al(1)-O(3) 102.58(17); O(1)^{1}-Al(1)-O(1)^{2} 154.8(2); O(1)^{1}-Al(1)-O(1)^{3} 87.08(18); O(1)^{1}-Al(1)-O(3) 102.58(17); O(1)^{2}-Al(1)-O(1)^{3} 87.5(2); O(1)^{2}-Al(1)-O(3) 102.58(17); O(1)^{3}-Al(1)-O(3) 102.58(17); W(1)-O(1)-W(1)^{11} 140.7(3); W(1)-O(1)-Al(1)^{11} 140.7(3); W(1)^{11}-O(1)-Al(1) 140.7(3); Al(1)-O(1)-Al(1)^{11} 140.7(3); W(1)-O(2)-W(1)^{11} 91.97(16); W(1)-O(2)-W(1)^{12} 91.97(16); W(1)-O(2)-P(1) 123.9(3); W(1)-O(2)-O(2)^{7} 131.4(3); W(1)-O(2)-O(2)^{4} 69.1(3); W(1)-O(2)-O(2)^{10} 131.4(3); W(1)^{11}-O(2)-W(1)^{12} 91.97(16); W(1)^{11}-O(2)-P(1) 123.9(3); W(1)^{11}-O(2)-O(2)^{7} 69.1(3) W(1)^{11}-O(2)-O(2)^{4} 131.4(3); W(1)^{11}-O(2)- O(2)^{10} 131.4(3); W(1)^{12}-O(2)-P(1) 123.9(3); W(1)^{12}-O(2)-O(2)^{7} 131.4(3); W(1)^{12}-O(2)-O(2)^{4} 131.4(3); W(1)^{12}-O(2)-O(2)^{10} 69.1(3); P(1)-O(2)-O(2)^{7} 54.7(3); P(1)-O(2)-O(2)^{4} 54.7(3); P(1)-O(2)-O(2)^{10} 54.7(3); O(2)^{7}-O(2)-O(2)^{4} 90.0(3); O(2)^{7}-O(2)-O(2)^{10} 90.0(3); O(2)^{4}-O(2)-O(2)^{10} 90.0(3). Symmetry operators: (1) X,Z,Y (2) Z,Y,-X+1 (3) Z,-X+1,Y (4) Y,Z,-X+1 (5) Y,Z,X (6) Z,X,Y (7) X,Y,-Z+1 (8) Z,X,-Y+1 (9) -Z+1,X,-Y+1 (10) -Y+1,-Z+1,-X+1 (11) -Y+1,Z,-X+1 (12) -Z+1,-X+1,Y.

7. References

Akitt, J. W. (1988). Multinuclear Studies of Aluminum Compounds. *Prog. Nucl. Magn. Res. Spectr.*,Vol.21, No.1-2, pp. 1–149

Baes, C. F. Jr. & Mesmer, R. E. (1976). *The Hydrolysis of Cations*, pp. 112–123, John Wiley, New York, 1976

Busbongthong, S. & Ozeki, T. (2009). Structural Relationships among Methyl-, Dimethyl-, and Trimethylammonium Phosphdodecatungstates. *Bull. Chem. Soc. Jpn.*, Vol.82, No.11, pp. 1393–1397

Contant, R. (1987). Relation between Tungstophosphates Related to the Phosphorus Tungsten Oxide Anion ($PW_{12}O_{40}^{3-}$). Synthesis and Properties of a New Lacunary Potassium Polytungstophosphate ($K_{10}P_2W_{20}O_{70}\cdot 24H_2O$). *Can. J. Chem.*, Vol.65, No.3, pp. 568–573

Cotton, F. A. & Wilkinson, G. (1988). *Advanced Inorganic Chemistry, Fifth Edition*, John Wiley & Sons, New York

Djurdjevic P.; Jelic, R. & Dzajevic, D. (2000). The Effect of Surface Active Substances on Hydrolysis of Aluminum(III) Ion. *Main Metal Chemistry*, Vol.23, No.8, pp. 409–421

Domaille, P. J. (1990). Vanadium(V) Substituted Dodecatungstophosphates. *Inorg. Synth.*, Vol.27, pp. 96–104

Frisch, M. J.; Trucks, G. W.; Schlegel, H. B.; Scuseria, G. E.; Robb, M. A.; Cheeseman, J. R.; Scalmani, G.; Barone, V.; Mennucci, B.; Petersson, G. A.; Nakatsuji, H.; Caricato, M.; Li, X.; Hratchian, H. P.; Izmaylov, A. F.; Bloino, J.; Zheng, G.; Sonnenberg, J. L.; Hada, M.; Ehara, M.; Toyota, K.; Fukuda, R.; Hasegawa, J.; Ishida, M.; Nakajima, T.; Honda, Y.; Kitao, O.; Nakai, H.; Vreven, T.; Montgomery, Jr., J. A.; Peralta, J. E.; Ogliaro, F.; Bearpark, M.; Heyd, J. J.; Brothers, E.; Kudin, K. N.; Staroverov, V. N.; Kobayashi, R.; Normand, J.; Raghavachari, K.; Rendell, A.; Burant, J. C.; Iyengar, S. S.; Tomasi, J.; Cossi, M.; Rega, N.; Millam, N. J.; Klene, M.; Knox, J. E.; Cross, J. B.; Bakken, V.; Adamo, C.; Jaramillo, J.; Gomperts, R.; Stratmann, R. E.; Yazyev, O.; Austin, A. J.; Cammi, R.; Pomelli, C.; Ochterski, J. W.; Martin, R. L.; Morokuma, K.; Zakrzewski, V. G.; Voth, G. A.; Salvador, P.; Dannenberg, J. J.; Dapprich, S.; Daniels, A. D.; Farkas, Ö.; Foresman, J. B.; Ortiz, J. V.; Cioslowski, J. & Fox, D. J. (2009). *Gaussian 09, Revision B.1*, Gaussian, Inc., Wallingford CT

Fukaya, K.; Srifa, A.; Ishikawa, E. & Naruke, H. (2010). Synthesis and Structural Characterization of Polyoxometalates Incorporating with Anilinium Cations and Facile Preparation of Hybrid Film. *J. Mol. Struc.* Vol.979, pp. 221–226

Hou, Y.; Fang, X. & Hill, C. L. (2007). Breaking Symmetry: Spontaneous Resolution of a Polyoxometalate. *Chem. Eur. J.* Vol.13, pp. 9442–9447

Kato, C. N.; Hara, K.; Kato, M.; Amano, H.; Sato, K.; Kataoka, Y. & Mori, W. (2010). EDTA-Reduction of Water to Molecular Hydrogen Catalyzed by Visible-Light-Response TiO_2-Based Materials Sensitized by Dawson- and Keggin-Type Rhenium(V)-Containing Polyoxotungstates. *Materials*, Vol.3, pp. 897–917

Kato, C. N.; Katayama, Y.; Nagami, M.; Kato, M. & Yamasaki, M. (2010). A Sandwich-type Aluminium Complex Composed of Tri-lacunary Keggin-type Polyoxotungstate: Synthesis and X-Ray Crystal Structure of $[(A\text{-}PW_9O_{34})_2\{W(OH)(OH_2)\}\text{-}\{Al(OH)(OH_2)\}\{Al(\mu\text{-}OH)(OH_2)_2\}_2]^{7-}$. *Dalton Trans.*, Vol.39, pp. 11469–11474

Kikukawa, Y.; Yamaguchi, S.; Nakagawa, Y.; Uehara, K.; Uchida, S.; Yamaguchi, K. & Mizuno, N. (2008). Synthesis of a Dialuminum-Substituted Silicotungstate and the Diasteroselective Cyclization of Citronellal Derivatives. *J. Am. Chem. Soc.*, Vol.130, No.47, 15872–15878

Knoth, W. H.; Domaille, P. J. & Roe, D. C. (1983). Halometal Derivatives of $W_{12}PO_{40}^{3-}$ and Related ^{183}W NMR Studies. *Inorg. Chem.* Vol.22, 198–201

Knoth, W. H. & Harlow, R. L. (1981). New Tungstophosphates: $Cs_6W_5P_2O_{23}$, $Cs_7W_{10}PO_{36}$, and $Cs_7Na_2W_{10}PO_{37}$. *J. Am. Chem. Soc.*, Vol.103. No.7, pp. 1865–1867

Lin, Y.; Weakley, T. J. R.; Rapko, B. & Finke, R. G. (1993). Polyoxoanions Derived from Tungstosilicatie ($A\text{-}\beta\text{-}SiW_9O_{34}^{10-}$): Synthesis, Single-crystal Structural Determination, and Solution Structural Characterization by Tungsten-183 NMR and IR of Titanotungstosilicate ($A\text{-}\beta\text{-}Si_2W_{18}Ti_6O_{77}^{14-}$). *Inorg. Chem.*, Vol.32, No.23, pp. 5095–5101

Maestre, J. M.; Lopez, X.; Bo, C.; Poblet, J.-M. & Casan-Pastor N. (2001). Electronic and Magnetic Properties of α-Keggin Anions: A DFT Study of $[XM_{12}O_{40}]^{n-}$, (M = W, Mo; X = Al^{III}, Si^{VI}, P^{V}, Fe^{III}, Co^{II}, Co^{III}) and $[SiM_{11}VO_{40}]^{m-}$ (M = Mo and W). *J. Am. Chem. Soc.*, Vol.123, pp. 3749–3758

Neiwert, W. A.; Cowan, J. J.; Hardcastle, K. I.; Hill, C. L. & Weinstock, I. A. (2002). Stability and Structure in α- and β-Keggin Heteropolytungstates, $[X^{n+}W_{12}O_{40}]^{(8-n)-}$, X = *p*-Block Cation. *Inorg. Chem.*, Vol.41, 6950–6952

Nomiya, K.; Takahashi, M.; Ohsawa, K. & Widegren, J. A. (2001). Synthesis and Characterization of Tri-titanium(IV)-1,2,3-substituted α-Keggin Polyoxotungstates with Heteroatoms P and Si. Crystal Structure of the Dimeric, Ti-O-Ti Bridged Anhydride Form $K_{10}H_2[\alpha,\alpha\text{-}P_2W_{18}Ti_6O_{77}]\cdot 17H_2O$ and Confirmation of Dimeric Forms in Aqueous Solution by Ultracentrifugation Molecular Weight Measurements. *J. Chem. Soc., Dalton Trans.* No.19, pp. 2872-2878

Nomiya, K.; Takahashi, M. Widegren, J. A.; Aizawa, T.; Sakai, Y. & Kasuga, N. C. (2002). Synthesis and pH-Variable Ultracentrifugation Molecular Weight Measurements of the Dimeric, Ti-O-Ti Bridged Anhydride Form of a Novel Di-Ti^{IV}-substituted α-Keggin Polyoxotungstate. Molecular Structure of the $[(\alpha\text{-}1,2\text{-}PW_{10}Ti_2O_{39})_2]^{10-}$ Polyoxoanion. *J. Chem. Soc., Dalton Trans.* No.19, pp. 3679–3685

Ortéga, F.; Pope, M. T. & Evans, H.T., Jr. (1997). Tungstorhenate Heteropolyanions. 2. Synthesis and Characterization of Enneatungstorhebates(V), -(VI) and -(VII). *Inorg. Chem.*, Vol.36, No.10, pp. 2166–2169

Orvig, C. (1993). The Aqueous Coordination Chemistry of Aluminum In: *Coordination Chemistry of Aluminum*, G.H. Robinson, (Ed.), 85–121, VCH, Weinheim

Patel, K.; Shringarpure, P. & Patel, A. (2011). One-step Synthesis of a Keggin-type Manganese(II)-substitited Phosphotungstate: Structrural and Spectroscopic

Characterization and Non-solvent Liquid Phase Oxidation of Styrene. *Transition Met. Chem.*, Vol.36, pp. 171–177

Pope, M. T. (1983). *Heteropoly and Isopoly Oxometalates*, Springer-Verlag, Berlin

Pope, M. T. & Müller, A. (1991). Chemistry of Polyoxometallates. Actual Variation on an Old Theme with Interdisciplinary References. *Angew. Chem. Int. Ed. Engl.*, Vol.30, No.1, pp. 34–48

Pope, M. T. & Müller, A. (Eds.), (1994). *Polyoxometalates: From Platonic Solids to Anti-Retroviral Activity,* Kluwer Academic Publishers, Dordrecht, The Netherlands

Reinoso, S.; Vitoria, P.; Felices, L. S.; Lezama, L. & Gutiérrez-Zorrilla, J. M. (2006). Analysis of Weak Interactions in the Crystal Packing of Inorganic Metalorganic Hybrids Based on Keggin Polyoxometalates and Dinuclear Copper(II)-Acetate Complexes. *Inorg. Chem.*, Vol.45, pp. 108–118

Rocchiccioli-Deltcheff, C.; Fournier, M.; Franck, R. & Thouvenot, R. (1983). Vibrational Investigations of Polyoxometalates. 2. Evidence for Anion-Anion Interactions in Molybdenum(VI) and Tungsten(VI) Compounds Related to the Keggin Structure. *Inorg. Chem.*, Vol.22, pp. 207–216

Rosenheim, A. & Jaenicke, J. *Z.* (1917). Iso- and Heteropoly Acids. XV. Heteropoly tungstates and Some Heteropoly Molybdates. *Anorg. Allg. Chem.*, Vol.101, pp. 235–275

Shannon, R. D. (1976). Revised Effective Ionic Radii and Systematic Studies of Interatomic Distances in Halides and Chalcogenides. *Acta Crystallogr., Sect. A*, Vol.A32, pp. 751–767

Sheldrick, G. M. (2008). A Short History of SHELX. *Acta Crystallogr., Sect. A*, Vol.A46, No.1, pp. 112–122

Spek, A. L. (2009). Structure Validation in Chemical Crystallography. *Acta Crystallogr., Sect. D*, Vol.D65, No.2, pp. 148–155

Thouvenot, R.; Fournier, M.; Franck, R. & Rocchiccioli-Deltcheff, C. (1984). Vibrational Investigations of Polyoxometalates. 3. Isomerism in Molybdenum(VI) and Tungsten(VI) Compounds Related to the Keggin Structure. *Inorg. Chem.*, Vol.23, pp. 598–605

Weakley, T. J. R. (1987). Crystal Structure of Cesium Aquanickelo(II)undecatungstophsphate Dihydrate. J. Cryst. Spectro. Res., Vol.17, No.3, pp. 383–391

Weakley, T. J. R. & Finke, R. G. (1990). Single-crystal X-Ray Structures of the Polyoxotungstate Salts $K_{8.3}Na_{1.7}[Cu_4(H_2O)_2(PW_9O_{34})_2]\cdot 24H_2O$ and $Na_{14}Cu[Cu_4(H_2O)_2(P_2W_{15}O_{56})_2]\cdot 53H_2O$. *Inorg. Chem.*, Vol.29, No.6, pp. 1235–1241

Weiner, H.; Aiken III, J. D. & Finke, R. G. (1996). Polyoxometalate Catalyst Precursors. Improved Synthesis, H^+-Titration Procedure, and Evidence for ^{31}P NMR as a Highly Sensitive Support-Site Indicator for the Prototype Polyoxoanion-Organometallic-support System $[(n\text{-}C_4H_9)_4N]_9P_2W_{15}Nb_3O_{62}$. *Inorg. Chem.*, Vol.35, pp. 7905–7913

Yang, Q. H.; Zhou, D. F.; Dai, H. C.; Liu, J. F.; Xing, Y.; Lin, Y. H. & Jia, H. Q. (1997). Synthesis, Structure and Properties of Undecatungstozincate Containing 3A Elements. *Polyhedron*, Vol.16, No.23, 3985–3989

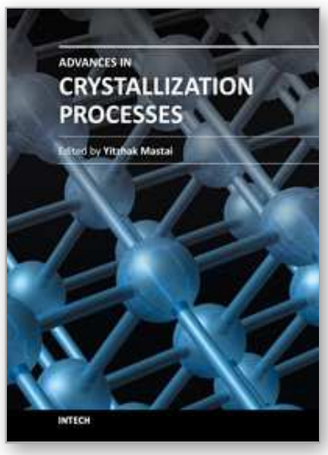

Advances in Crystallization Processes
Edited by Dr. Yitzhak Mastai

ISBN 978-953-51-0581-7
Hard cover, 648 pages
Publisher InTech
Published online 27, April, 2012
Published in print edition April, 2012

Crystallization is used at some stage in nearly all process industries as a method of production, purification or recovery of solid materials. In recent years, a number of new applications have also come to rely on crystallization processes such as the crystallization of nano and amorphous materials. The articles for this book have been contributed by the most respected researchers in this area and cover the frontier areas of research and developments in crystallization processes. Divided into five parts this book provides the latest research developments in many aspects of crystallization including: chiral crystallization, crystallization of nanomaterials and the crystallization of amorphous and glassy materials. This book is of interest to both fundamental research and also to practicing scientists and will prove invaluable to all chemical engineers and industrial chemists in the process industries as well as crystallization workers and students in industry and academia.

InTech Europe
University Campus STeP Ri
Slavka Krautzeka 83/A
51000 Rijeka, Croatia
Phone: +385 (51) 770 447
Fax: +385 (51) 686 166
www.intechopen.com

InTech China
Unit 405, Office Block, Hotel Equatorial Shanghai
No.65, Yan An Road (West), Shanghai, 200040, China
中国上海市延安西路65号上海国际贵都大饭店办公楼405单元
Phone: +86-21-62489820
Fax: +86-21-62489821

IntechOpen